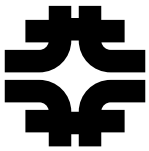

Fermi National Accelerator Laboratory

FERMILAB-Pub-97/106-E
CDF

Properties of Photon Plus Two-Jet Events in $\bar{p}p$ Collisions at $\sqrt{s}$ = 1.8 TeV

F. Abe et al.
The CDF Collaboration

Fermi National Accelerator Laboratory
P.O. Box 500, Batavia, Illinois 60510

April 1997

Submitted to *Physical Review D*

Operated by Universities Research Association Inc. under Contract No. DE-AC02-76CH03000 with the United States Department of Energy

Disclaimer

Distribution

Properties of Photon Plus Two-Jet Events in $\bar{p}p$ Collisions at $\sqrt{s} = 1.8$ TeV

April 22, 1997

F. Abe,[17] H. Akimoto,[36] A. Akopian,[31] M. G. Albrow,[7] S. R. Amendolia,[27] D. Amidei,[20] J. Antos,[33] S. Aota,[36] G. Apollinari,[31] T. Asakawa,[36] W. Ashmanskas,[18] M. Atac,[7] F. Azfar,[26] P. Azzi-Bacchetta,[25] N. Bacchetta,[25] W. Badgett,[20] S. Bagdasarov,[31] M. W. Bailey,[22] J. Bao,[39] P. de Barbaro,[30] A. Barbaro-Galtieri,[18] V. E. Barnes,[29] B. A. Barnett,[15] M. Barone,[9] E. Barzi,[9] G. Bauer,[19] T. Baumann,[11] F. Bedeschi,[27] S. Behrends,[3] S. Belforte,[27] G. Bellettini,[27] J. Bellinger,[38] D. Benjamin,[35] J. Benlloch,[19] J. Bensinger,[3] D. Benton,[26] A. Beretvas,[7] J. P. Berge,[7] J. Berryhill,[5] S. Bertolucci,[9] B. Bevensee,[26] A. Bhatti,[31] K. Biery,[7] M. Binkley,[7] D. Bisello,[25] R. E. Blair,[1] C. Blocker,[3] A. Bodek,[30] W. Bokhari,[19] V. Bolognesi,[2] G. Bolla,[29] D. Bortoletto,[29] J. Boudreau,[28] L. Breccia,[2] C. Bromberg,[21] N. Bruner,[22] E. Buckley-Geer,[7] H. S. Budd,[30] K. Burkett,[20] G. Busetto,[25] A. Byon-Wagner,[7] K. L. Byrum,[1] J. Cammerata,[15] C. Campagnari,[7] M. Campbell,[20] A. Caner,[27] W. Carithers,[18] D. Carlsmith,[38] A. Castro,[25] D. Cauz,[27] Y. Cen,[30] F. Cervelli,[27] P. S. Chang,[33] P. T. Chang,[33] H. Y. Chao,[33] J. Chapman,[20] M. -T. Cheng,[33] G. Chiarelli,[27] T. Chikamatsu,[36] C. N. Chiou,[33] L. Christofek,[13] S. Cihangir,[7] A. G. Clark,[10] M. Cobal,[27] E. Cocca,[27] M. Contreras,[5] J. Conway,[32] J. Cooper,[7] M. Cordelli,[9] C. Couyoumtzelis,[10] D. Crane,[1] D. Cronin-Hennessy,[6] R. Culbertson,[5] T. Daniels,[19] F. DeJongh,[7] S. Delchamps,[7] S. Dell'Agnello,[27] M. Dell'Orso,[27] R. Demina,[7] L. Demortier,[31] M. Deninno,[2] P. F. Derwent,[7] T. Devlin,[32] J. R. Dittmann,[6] S. Donati,[27] J. Done,[34] T. Dorigo,[25] A. Dunn,[20] N. Eddy,[20] K. Einsweiler,[18] J. E. Elias,[7] R. Ely,[18] E. Engels, Jr.,[28] D. Errede,[13] S. Errede,[13] Q. Fan,[30] G. Feild,[39] C. Ferretti,[27]

I. Fiori,[2] B. Flaugher,[7] G. W. Foster,[7] M. Franklin,[11] M. Frautschi,[35] J. Freeman,[7] J. Friedman,[19] H. Frisch,[5] Y. Fukui,[17] S. Funaki,[36] S. Galeotti,[27] M. Gallinaro,[26] O. Ganel,[35] M. Garcia-Sciveres,[18] A. F. Garfinkel,[29] C. Gay,[11] S. Geer,[7] D. W. Gerdes,[15] P. Giannetti,[27] N. Giokaris,[31] P. Giromini,[9] G. Giusti,[27] L. Gladney,[26] D. Glenzinski,[15] M. Gold,[22] J. Gonzalez,[26] A. Gordon,[11] A. T. Goshaw,[6] Y. Gotra,[25] K. Goulianos,[31] H. Grassmann,[27] L. Groer,[32] C. Grosso-Pilcher,[5] G. Guillian,[20] R. S. Guo,[33] C. Haber,[18] E. Hafen,[19] S. R. Hahn,[7] R. Hamilton,[11] R. Handler,[38] R. M. Hans,[39] F. Happacher,[9] K. Hara,[36] A. D. Hardman,[29] B. Harral,[26] R. M. Harris,[7] S. A. Hauger,[6] J. Hauser,[4] C. Hawk,[32] E. Hayashi,[36] J. Heinrich,[26] B. Hinrichsen,[14] K. D. Hoffman,[29] M. Hohlmann,[5] C. Holck,[26] R. Hollebeek,[26] L. Holloway,[13] S. Hong,[20] G. Houk,[26] P. Hu,[28] B. T. Huffman,[28] R. Hughes,[23] J. Huston,[21] J. Huth,[11] J. Hylen,[7] H. Ikeda,[36] M. Incagli,[27] J. Incandela,[7] G. Introzzi,[27] J. Iwai,[36] Y. Iwata,[12] H. Jensen,[7] U. Joshi,[7] R. W. Kadel,[18] E. Kajfasz,[25] H. Kambara,[10] T. Kamon,[34] T. Kaneko,[36] K. Karr,[37] H. Kasha,[39] Y. Kato,[24] T. A. Keaffaber,[29] K. Kelley,[19] R. D. Kennedy,[7] R. Kephart,[7] P. Kesten,[18] D. Kestenbaum,[11] H. Keutelian,[7] F. Keyvan,[4] B. Kharadia,[13] B. J. Kim,[30] D. H. Kim,[7a] H. S. Kim,[14] S. B. Kim,[20] S. H. Kim,[36] Y. K. Kim,[18] L. Kirsch,[3] P. Koehn,[23] K. Kondo,[36] J. Konigsberg,[8] S. Kopp,[5] K. Kordas,[14] A. Korytov,[8] W. Koska,[7] E. Kovacs,[7a] W. Kowald,[6] M. Krasberg,[20] J. Kroll,[7] M. Kruse,[30] T. Kuwabara,[36] S. E. Kuhlmann,[1] E. Kuns,[32] A. T. Laasanen,[29] S. Lami,[27] S. Lammel,[7] J. I. Lamoureux,[3] M. Lancaster,[18] T. LeCompte,[1] S. Leone,[27] J. D. Lewis,[7] P. Limon,[7] M. Lindgren,[4] T. M. Liss,[13] J. B. Liu,[30] Y. C. Liu,[33] N. Lockyer,[26] O. Long,[26]

C. Loomis,[32] M. Loreti,[25] J. Lu,[34] D. Lucchesi,[27] P. Lukens,[7] S. Lusin,[38] J. Lys,[18] K. Maeshima,[7] A. Maghakian,[31] P. Maksimovic,[19] M. Mangano,[27] J. Mansour,[21] M. Mariotti,[25] J. P. Marriner,[7] A. Martin,[39] J. A. J. Matthews,[22] R. Mattingly,[19] P. McIntyre,[34] P. Melese,[31] A. Menzione,[27] E. Meschi,[27] S. Metzler,[26] C. Miao,[20] T. Miao,[7] G. Michail,[11] R. Miller,[21] H. Minato,[36] S. Miscetti,[9] M. Mishina,[17] H. Mitsushio,[36] T. Miyamoto,[36] S. Miyashita,[36] N. Moggi,[27] Y. Morita,[17] A. Mukherjee,[7] T. Muller,[16] P. Murat,[27] H. Nakada,[36] I. Nakano,[36] C. Nelson,[7] D. Neuberger,[16] C. Newman-Holmes,[7] C-Y. P. Ngan,[19] M. Ninomiya,[36] L. Nodulman,[1] S. H. Oh,[6] K. E. Ohl,[39] T. Ohmoto,[12] T. Ohsugi,[12] R. Oishi,[36] M. Okabe,[36] T. Okusawa,[24] R. Oliveira,[26] J. Olsen,[38] C. Pagliarone,[27] R. Paoletti,[27] V. Papadimitriou,[35] S. P. Pappas,[39] N. Parashar,[27] S. Park,[7] A. Parri,[9] J. Patrick,[7] G. Pauletta,[27] M. Paulini,[18] A. Perazzo,[27] L. Pescara,[25] M. D. Peters,[18] T. J. Phillips,[6] G. Piacentino,[27] M. Pillai,[30] K. T. Pitts,[7] R. Plunkett,[7] L. Pondrom,[38] J. Proudfoot,[1] F. Ptohos,[11] G. Punzi,[27] K. Ragan,[14] D. Reher,[18] A. Ribon,[25] F. Rimondi,[2] L. Ristori,[27] W. J. Robertson,[6] T. Rodrigo,[27] S. Rolli,[37] J. Romano,[5] L. Rosenson,[19] R. Roser,[13] T. Saab,[14] W. K. Sakumoto,[30] D. Saltzberg,[5] A. Sansoni,[9] L. Santi,[27] H. Sato,[36] P. Schlabach,[7] E. E. Schmidt,[7] M. P. Schmidt,[39] A. Scribano,[27] S. Segler,[7] S. Seidel,[22] Y. Seiya,[36] G. Sganos,[14] M. D. Shapiro,[18] N. M. Shaw,[29] Q. Shen,[29] P. F. Shepard,[28] M. Shimojima,[36] M. Shochet,[5] J. Siegrist,[18] A. Sill,[35] P. Sinervo,[14] P. Singh,[28] J. Skarha,[15] K. Sliwa,[37] F. D. Snider,[15] T. Song,[20] J. Spalding,[7] T. Speer,[10] P. Sphicas,[19] F. Spinella,[27] M. Spiropulu,[11] L. Spiegel,[7] L. Stanco,[25] J. Steele,[38] A. Stefanini,[27] K. Strahl,[14] J. Strait,[7]

R. Ströhmer,[7a] D. Stuart,[7] G. Sullivan,[5] K. Sumorok,[19] J. Suzuki,[36] T. Takada,[36] T. Takahashi,[24] T. Takano,[36] K. Takikawa,[36] N. Tamura,[12] B. Tannenbaum,[22] F. Tartarelli,[27] W. Taylor,[14] P. K. Teng,[33] Y. Teramoto,[24] S. Tether,[19] D. Theriot,[7] T. L. Thomas,[22] R. Thun,[20] R. Thurman-Keup,[1] M. Timko,[37] P. Tipton,[30] A. Titov,[31] S. Tkaczyk,[7] D. Toback,[5] K. Tollefson,[30] A. Tollestrup,[7] H. Toyoda,[24] W. Trischuk,[14] J. F. de Troconiz,[11] S. Truitt,[20] J. Tseng,[19] N. Turini,[27] T. Uchida,[36] N. Uemura,[36] F. Ukegawa,[26] G. Unal,[26] J. Valls,[7a] S. C. van den Brink,[28] S. Vejcik, III,[20] G. Velev,[27] R. Vidal,[7] R. Vilar,[7a] M. Vondracek,[13] D. Vucinic,[19] R. G. Wagner,[1] R. L. Wagner,[7] J. Wahl,[5] N. B. Wallace,[27] A. M. Walsh,[32] C. Wang,[6] C. H. Wang,[33] J. Wang,[5] M. J. Wang,[33] Q. F. Wang,[31] A. Warburton,[14] T. Watts,[32] R. Webb,[34] C. Wei,[6] H. Wenzel,[16] W. C. Wester, III,[7] A. B. Wicklund,[1] E. Wicklund,[7] R. Wilkinson,[26] H. H. Williams,[26] P. Wilson,[5] B. L. Winer,[23] D. Winn,[20] D. Wolinski,[20] J. Wolinski,[21] S. Worm,[22] X. Wu,[10] J. Wyss,[25] A. Yagil,[7] W. Yao,[18] K. Yasuoka,[36] Y. Ye,[14] G. P. Yeh,[7] P. Yeh,[33] M. Yin,[6] J. Yoh,[7] C. Yosef,[21] T. Yoshida,[24] D. Yovanovitch,[7] I. Yu,[7] L. Yu,[22] J. C. Yun,[7] A. Zanetti,[27] F. Zetti,[27] L. Zhang,[38] W. Zhang,[26] and S. Zucchelli[2]

(CDF Collaboration)

[1] *Argonne National Laboratory, Argonne, Illinois 60439*

[2] *Istituto Nazionale di Fisica Nucleare, University of Bologna, I-40127 Bologna, Italy*

[3] *Brandeis University, Waltham, Massachusetts 02264*

[4] *University of California at Los Angeles, Los Angeles, California 90024*

[5] *University of Chicago, Chicago, Illinois 60638*

[6] *Duke University, Durham, North Carolina 28708*

[7] *Fermi National Accelerator Laboratory, Batavia, Illinois 60510*

[8] *University of Florida, Gainesville, FL 33611*

[9] *Laboratori Nazionali di Frascati, Istituto Nazionale di Fisica Nucleare, I-00044 Frascati, Italy*

[10] *University of Geneva, CH-1211 Geneva 4, Switzerland*

[11] *Harvard University, Cambridge, Massachusetts 02138*

[12] *Hiroshima University, Higashi-Hiroshima 724, Japan*

[13] *University of Illinois, Urbana, Illinois 61801*

[14] *Institute of Particle Physics, McGill University, Montreal H3A 2T8, and University of Toronto, Toronto M5S 1A7, Canada*

[15] *The Johns Hopkins University, Baltimore, Maryland 21218*

[16] *Universotät Karlsruhe, 76128 Karlsruhe, Germany*

[17] *National Laboratory for High Energy Physics (KEK), Tsukuba, Ibaraki 315, Japan*

[18] *Ernest Orlando Lawrence Berkeley National Laboratory, Berkeley, California 94720*

[19] *Massachusetts Institute of Technology, Cambridge, Massachusetts 02139*

[20] *University of Michigan, Ann Arbor, Michigan 48109*

[21] *Michigan State University, East Lansing, Michigan 48824*

[22] *University of New Mexico, Albuquerque, New Mexico 87132*

[23] *The Ohio State University, Columbus, OH 43320*

[24] *Osaka City University, Osaka 588, Japan*

[25] *Universita di Padova, Istituto Nazionale di Fisica Nucleare, Sezione di Padova, I-36132 Padova, Italy*

[26] *University of Pennsylvania, Philadelphia, Pennsylvania 19104*

[27] *Istituto Nazionale di Fisica Nucleare, University and Scuola Normale Superiore of Pisa, I-56100 Pisa, Italy*

[28] *University of Pittsburgh, Pittsburgh, Pennsylvania 15270*

[29] *Purdue University, West Lafayette, Indiana 47907*

[30] *University of Rochester, Rochester, New York 14628*

[31] *Rockefeller University, New York, New York 10021*

[32] *Rutgers University, Piscataway, New Jersey 08854*

[33] *Academia Sinica, Taipei, Taiwan 11530, Republic of China*

[34] *Texas A&M University, College Station, Texas 77843*

[35] *Texas Tech University, Lubbock, Texas 79409*

[36] *University of Tsukuba, Tsukuba, Ibaraki 315, Japan*

[37] *Tufts University, Medford, Massachusetts 02155*

[38] *University of Wisconsin, Madison, Wisconsin 53806*

[39] *Yale University, New Haven, Connecticut 06511*

Abstract

We present the first general measurements (invariant-mass, transverse-energy, and angular distributions) of the process, $\bar{p}p \rightarrow \gamma + 2\,\mathrm{Jets} + \mathrm{X}$, using data collected by CDF at Fermilab. We compare the data with predictions from a tree-level QCD calculation and the PYTHIA shower Monte Carlo. Our data sample is particularly sensitive to contributions from initial- and final-state radiation of photons and jets. Using the PYTHIA Monte Carlo, we contrast the kinematical distributions for direct photon production with those for initial- and final-state photon radiation (bremsstrahlung). Based on the angular distributions, we find that our data favor a mixture of bremsstrahlung and direct photon production, as predicted, over either process alone.

Pacs 13.85.Qk 13.85.Hd

I. INTRODUCTION

Measurements of prompt photon production provide good tests for the predictions of perturbative Quantum Chromodynamics (QCD) [1]. This paper presents the first measurements of hadronic production of prompt photon plus two-or-more jets in the final state. These measurements were carried out using the Collider Detector at Fermilab (CDF). The data sample corresponds to an integrated luminosity of 16 pb^{-1} [2] at $\sqrt{s} = 1.8$ TeV.

There are two main motivations for studying this final state. First, we wish to understand how well the general features of this final state are predicted by current QCD calculations. For this purpose, we have compared the data with two very different models, a full tree-level calculation [3] of the photon plus two-parton system, and the PYTHIA parton-shower Monte Carlo [4]. Second, this final state provides direct access for the first time to the bremsstrahlung production process. The distinction between bremsstrahlung and direct production is illustrated in Fig. 1; Figs. 1a and 1b are examples of direct production, while Fig. 1c illustrates bremsstrahlung radiation off a final-state quark line. Although the rate for photon radiation is small compared to gluon radiation, the dijet-production cross section is sufficiently large that bremsstrahlung production is predicted to be of the same order as direct production. Within the framework of PYTHIA, we investigate the relative rates for bremsstrahlung and direct photon production. In particular, this investigation may shed light on the inclusive photon cross

section measured at the Tevatron, which shows an excess at low transverse momentum over next-to-leading order ($\mathcal{O}(\alpha_{\rm em}\alpha_s^2)$) QCD calculations [5, 6]. Although this excess may be explained by parton-shower effects [7], there are uncertainties associated with this kind of calculation. Part of the excess could still come from another source. The bremsstrahlung process, for example, introduces a significant number of diagrams to inclusive photon production for the first time at $\mathcal{O}(\alpha_{\rm em}\alpha_s^2)$, and it is conceivable that the next-order contributions may be important too. Thus, the study of bremsstrahlung production in the photon plus two-jet system should help to illuminate the bremsstrahlung contributions to inclusive prompt-photon production.

The structure of this paper is as follows. In Sec. II we describe the data selection, including background subtractions and experimental systematic uncertainties. In Sec. III we describe the QCD predictions. In Sec. IV we present the kinematic comparison of data and theory, including theoretical uncertainties and their bearing on these comparisons. We also compare the bremsstrahlung and direct photon production processes within the PYTHIA framework. In Sec. V we summarize our conclusions on the study of photon plus two-jet final states.

II. Data Sample

Data were collected with the Collider Detector at Fermilab (CDF) in $\bar{p}p$ collisions at $\sqrt{s}$=1.8 TeV. A detailed description of CDF can be found elsewhere [8]. The primary components relevant to this analysis are those that measured photon and jet energies, and established the $\bar{p}p$ collision vertex.

Photons were detected in the central calorimeter, which spans 2π in azimuthal angle, ϕ, and subtends the pseudorapidity interval $|\eta| < 1.1$, where $\eta \equiv -\ln(\tan\theta/2)$ and θ is the polar angle from the proton beam direction. Calorimeter cells were divided into electromagnetic (EM) and hadronic (HAD) segments. Two additional detector elements were used specifically for photon identification: the central strip chamber (CES) embedded in the EM calorimeter at a depth near shower maximum and the central preradiator proportional chambers (CPR) located in front of the calorimeter. The full CDF calorimeter ($|\eta|$ <4) was used to identify jets. The event vertex was established with a set of time projection chambers located around the beam line.

The trigger required a photon candidate with a transverse energy, $\mathrm{E_T} \equiv E\sin\theta$, above a threshold of 16 GeV. The trigger also required that the candidate be isolated, with less than 4 GeV of additional calorimeter energy (EM+HAD) in a cone of $\Delta R < 0.7$ around the candidate ($\Delta R \equiv \sqrt{\Delta\eta^2 + \Delta\phi^2}$). In the offline analysis, photon candidates were required to have $|\eta| < 0.9$ and to pass standard fiducial cuts that guarantee sufficient shower containment in the CES and CPR chambers. Photon candidates with nearby

charged particles or additional photons (seen in the CES) were eliminated. Details of the photon analysis may be found in reference [9]. In addition, the event vertex was required to lie within 60 cm of the detector center. A total of 144000 inclusive photon-candidate events passed these selection criteria.

Jets were identified as clusters of energy in a cone of radius $\Delta R = 0.7$ [10]. The photon candidate events were required to have at least two additional jets with $E_T^{Jet} > 8$ GeV and $|\eta^{Jet}| < 2.5$, where η^{Jet} is the direction of the jet centroid. Photon and jet clusters were also required to be well separated ($\Delta R_{sep} \geq 0.8$). This photon candidate plus two-jets subsample contains 34116 events.

In this paper, the measured jet properties are not corrected for detector effects. Instead, comparisons are made (Section IV) to theoretical predictions that have been processed through the CDF detector simulation. While jet angles are well measured in the CDF calorimeters, jet energies are significantly affected by calorimeter non-hermeticity and nonlinearity. These effects are such that the calorimeter response to a jet with an E_T of 15 GeV would be 10.5 GeV on average. Taking resolution smearing and jet fragmentation into account as well, the 8 GeV jet E_T threshold used in this analysis corresponds to a parton E_T threshold of approximately 11 GeV. Note that these caveats do not apply to the photon candidates; photon energies are well measured.

A. BACKGROUND SUBTRACTION

Photon candidates consist of single photons and merged multiple photons from meson decays. The neutral-meson-background subtraction for prompt photons at CDF has been described in detail in ref. [9]. The CES measures transverse shower profiles, which for moderately low-energy (< 45 GeV) showers are narrower for single photons than for the neutral-meson decay products. The CPR counts photon conversions in the solenoid coil which has a thickness of 1.1 radiation lengths; the probability that an event contains a conversion is higher for the multiple photon background than for the single photon events. The probability that a candidate is a single photon is determined using CES (CPR) information for candidates below (above) 41 GeV in E_T. This probability is used to weight photon candidate events so as to provide an effective subtraction of meson backgrounds. The division between CES and CPR background-subtraction techniques is chosen to minimize the statistical uncertainty in the analysis. The neutral-meson background constitutes approximately 58% of the photon plus two-or-more-jet candidate sample. The inclusive-photon data at CDF contains a similar level of neutral-meson contamination [9].

After subtraction of meson decays, one further background to the sample was eliminated, namely prompt-photon plus two-jet events in which one or more jets were produced from a second hard scattering. This situation arises in events with a second $\bar{p}p$ collision or a second independent hard scattering within the primary $\bar{p}p$ collision. A

model of double-scatter processes was derived by combining CDF low-E_T jet events with inclusive-photon events, and then requiring the mixed events to pass our selection cuts. The level of double interactions in the photon plus two-or-more-jet event sample was estimated using conservation of transverse momentum. The momentum-vector sum of the photon and highest E_T jet was constructed, and the difference in the azimuthal angle ($\Delta\phi$) between this vector and the smaller E_T jet is shown in Fig. 2. Single scatter events populate this distribution near π as a result of momentum conservation; the distribution is smeared because of finite energy resolution and the possible presence of additional jets. Double-scatter events, on the other hand, are essentially flat in this variable since the two interactions are uncorrelated; the second scatter is randomly oriented in azimuth with respect to the first. Based on a two component fit to this distribution, using the double-scatter model and a prediction from the PYTHIA shower Monte Carlo (described below), the double-scatter contribution to our data sample is 14%. This measurement depends on the shape of the PYTHIA prediction. To eliminate this dependence, we note that the relatively flat double-scatter component is best observed in the tail of the distribution, at low $\Delta\phi$. In Fig. 2, we find that the tail, when interpreted entirely as double-scatter background, implies a background level of 28%. Systematic variations of the double-scatter model show that the level could be as high as 30%. We take this as the upper bound on the double-scatter contribution to our data set. Alternatively, if the tail predicted by PYTHIA is too small, all events at low $\Delta\phi$ may be single-scatter

events. We therefore assign the background to be $14^{+8}_{-7}\%$, so that $\pm 2\sigma$ spans the allowed range for background.

B. SYSTEMATIC UNCERTAINTY

The experimental systematic uncertainty is dominated by uncertainties in the double-scatter background and the jet-energy scale. The shape of the double-scatter background was determined for each measured distribution using the model derived from combining CDF events as described previously. The systematic uncertainty due to this background was determined by constructing two modified data samples: one with 22% ($+1\sigma$) background subtracted and another with 7% (-1σ) background subtracted. These different data sets show slightly different kinematic characteristics, which we take as a measure of systematic uncertainty.

The jet-energy scale uncertainty comes from a variety of effects ranging from fluctuations in parton fragmentation to the stability of the calorimeter response. A full discussion may be found in ref. [11]. We evaluated this experimental systematic uncertainty by selecting different data sets in which the jet energies were varied up and down one sigma ($^{+6}_{-9}\%$ at 8 GeV and $^{+3}_{-2}\%$ at 100 GeV). The resulting data samples show kinematic changes which are taken to represent the systematic uncertainty. Other sources of uncertainty include the jet-energy resolution, the photon isolation cuts, the neutral-meson background subtraction, and the vertex identification. These are all small compared to the two primary sources just described.

Given these experimental systematic uncertainties, the total number of photon plus two-or-more-jet events is $16900 \pm 300(\text{stat})^{+4100}_{-4500}(\text{sys})$ after correcting for neutral-meson and double-scatter backgrounds, trigger efficiency, efficiency of the extra photon cut [9] and efficiency for passing the isolation cut in the presence of a nearby jet.

III. QCD PREDICTIONS

We compare the data with two QCD predictions, a tree-level (TL) prediction of $\mathcal{O}(\alpha_{\rm em}\alpha_s^2)$ and the PYTHIA shower Monte Carlo. For the TL prediction, events with two initial- and three final-state partons from a $2\rightarrow3$ scattering were generated using the computational package of Owens[3] with the CTEQ2M [12] parton distribution functions, $\Lambda_{\rm QCD} = 0.213$ GeV, and a scale of $Q^2 = p_{\rm T}^2$, where $p_{\rm T} \equiv p\sin\theta$. Partons were fragmented into jets using a model from the ISAJET [13] Monte Carlo with fragmentation properties tuned using CDF data [10]. Resulting events were then passed through the detector simulation. The underlying event was included by combining the simulated TL event with a CDF event triggered on the $\bar{p}p$ bunch crossing only. Finally, photon- and jet-reconstruction algorithms were applied to these events. Reconstructed jets were required to come from a parton with $p_{\rm T} \geq 4$ GeV/c [14]. Simulated events that fail this cut account for less than 2% of the cross section and do not affect the kinematics of the sample.

The PYTHIA [4] (version 5.7) calculation generates $2\rightarrow2$ scatterings at leading order, and adds a coherent parton-shower model for radiation in the initial- and final-states.

To calculate direct photon production with PYTHIA, we generated all $2\rightarrow 2$ subprocesses with a final-state photon. To calculate the bremsstrahlung photons, we generated all quark and gluon $2\rightarrow 2$ subprocesses and accepted events with a photon produced in the subsequent radiation. All subprocesses were generated using the same parton distribution functions and Q^2 scale as in the TL calculation. The PYTHIA generator contains a fragmentation scheme and a model of the underlying event. After generation, PYTHIA photon events were passed through the detector simulation and CDF photon and jet reconstruction. The generator cuts were varied to ensure that the kinematic comparisons presented below are independent of the cuts.

IV. KINEMATIC COMPARISONS

Figures 3 and 4 show the primary kinematic distributions, namely the three-body invariant mass, the transverse-energy, and the angular correlation distributions for both data and QCD predictions. In order to facilitate the comparison of shapes, all distributions are normalized to unit area. The double-scatter background has been subtracted from the data in each plot. For illustrative purposes, the amount subtracted is shown as the shaded region at the bottom. The overall experimental systematic uncertainty is indicated by the shaded band surrounding the data.

General features of the data are reproduced by both predictions. In detail, however, deviations from the predictions are apparent. Figure 5 shows on a linear scale the

comparison of the data and the QCD predictions for the mass and E_T spectra. The three-body invariant mass spectrum is consistent with both models within the experimental systematic uncertainties. However, the photon and jet E_T spectra are generally softer than predicted by the models, and the photon spectrum, in particular, is inconsistent with either model, given the systematic uncertainties. We note that a similar effect is observed in inclusive photon production at CDF; the photon spectrum is systematically softer than the predictions of QCD [5]. The jet E_T spectra (Fig. 5c,d) are too soft to be consistent with the TL predictions; however, they are consistent with the PYTHIA predictions, within the systematic uncertainties. In the next section, we will discuss variations of the theoretical predictions that impact this comparison.

The azimuthal separations between the photon and jets are shown in Figs. 4a to 4c. In each case, Jet1 is the leading energy jet. Resolution smearing of the angular variables is small relative to the bin size in these plots. In all cases PYTHIA is consistent with our data within systematic uncertainty, while the TL simulation is not. The data show less correlation between the two jets than predicted by the TL simulation. The sensitivity of these distributions to variations of the TL prediction will be discussed in the next section.

The difference in pseudorapidity between the jets, $|\Delta\eta$(Jet1-Jet2)$|$, is shown in Fig. 4d. The distribution is similar to that which we obtain by plotting the difference of two random entries from the jet η distribution, implying that the jets are not strongly

correlated in η. Neither prediction describes the data in detail; the TL simulation is narrower and PYTHIA is wider. For PYTHIA, we find that the prediction depends on the implementation of color coherence in the first branching of a final-state shower [15]. The PYTHIA prediction with no final-state color coherence effects gives a $|\Delta\eta$(Jet1-Jet2)| distribution peaked more closely at zero, while leaving the other distributions unchanged.

A. THEORETICAL UNCERTAINTIES

As discussed above, there are a number of disagreements between the data and the theoretical predictions, which may reflect theoretical uncertainties. Empirically, we observe that in the case of the photon and jet transverse-energy distributions, the disagreements are significantly reduced by imposing a cut on the three-body invariant mass greater than 80 GeV/c^2. This is true for both the TL simulation and PYTHIA. *A priori*, we might expect this, since soft gluon resummation corrections at threshold are difficult to model. Other uncertainties that the TL simulation and PYTHIA have in common are the choice of the Q^2 scale and the parton distributions. We varied the Q^2 scale in the TL calculation from $p_{\rm T}^2$ to $p_{\rm T}^2/4$ and found negligible changes in the kinematic distributions. We varied the parton distributions from CTEQ2M to CTEQ2ML and CTEQ2MF [12] and again found negligible changes. While these reflect a broad range of parton distributions, they may not cover all possibilities. The disagreements, therefore, in transverse spectra between data and theory could in principle still be due to parton

distributions. The correct way to determine whether the parton distribution functions have enough freedom to account for the observed discrepancies would be to include these data in a QCD global fit such as performed in references [17, 18].

A number of theoretical uncertainties are unique to each prediction. PYTHIA does not have the full $2 \rightarrow 3$ matrix elements, and the approximations present in the parton-shower model have had only mixed success in the past in describing similar processes [19, 20]. The effect of changing various PYTHIA parameters to quantify this uncertainty is beyond the scope of this paper.

The TL calculation, by contrast, contains the full $2 \rightarrow 3$ matrix elements. However, this calculation makes no attempt to model higher-order radiations. We note that the inclusive photon spectrum measured at CDF, which is also softer than QCD predictions, is sensitive to a transverse boost tuned to model higher-order radiations [7]. Additionally, the TL calculation is followed by an independent-fragmentation scheme that is less physically motivated than PYTHIA's fragmentation. We have attempted to investigate these two uncertainties in the TL calculation.

One effect of higher-order radiation is the introduction of a transverse boost to the photon plus two-jet system. As a variation on the default calculation, a transverse boost, K_T, was added in an *ad hoc* fashion. This boost was tuned so that the transverse momentum of the photon plus two-jets system in the calculation matched the distribution observed in data (Fig. 6). Best agreement was found by adding a boost taken randomly

from a double-Gaussian distribution, 85% of which had a width of 7 GeV and 15% of which had a width of 12 GeV. The PYTHIA calculation includes a parton-shower model which adds a transverse boost to the three-body system. Figure 6 shows that PYTHIA's prediction is very similar to that observed in the data.

The effect of adding K_T to the TL calculation is shown in Figs. 7 and 8. It has the impact of flattening (or decorrelating) the angular distributions, but the changes to these distributions are not large. In particular, K_T broadens the $\Delta\phi$(Photon-Jet1) distribution, bringing it into closer agreement with the data. Agreement in the $\Delta\phi$ distributions involving Jet2, however, is not significantly improved. Figure 8 shows the effect of adding K_T on the mass and E_T spectra. To enhance the visibility of the effects, residual plots are shown. K_T is seen to soften the spectra, but again the changes are not large.

A second possible source of theoretical uncertainty is the fragmentation scheme used to convert the massless partons of the theory to jets of particles, which are by construction massive. This conversion is unphysical since momentum and energy cannot both be conserved. The default scheme assumes that the 3-vector sum of the momenta of the final-state particles is equal to the parton momentum. As a variation on this scheme, the parton-to-jets conversion was rescaled so that the scalar sum of the p_T's of the final-state particles is set equal to the parton p_T. As shown in Fig. 7c, this causes a systematic flattening of $\Delta\phi$(Jet1-Jet2) distribution, bringing it into closer agreement with the data.

The effects on the mass and E_T spectra are shown in Fig. 8. A greater softening is seen in the photon E_T spectrum than for the K_T variation. The softening in the photon spectrum is the result of a change in acceptance due to jet rescaling. The photon produced by the TL calculation is a final-state particle and is therefore not rescaled.

In all cases, variations due to K_T and fragmentation scheme either improve or leave unchanged the level of agreement between the TL prediction and data. Further sources of uncertainty are beyond the scope of this paper. Given the experimental and theoretical uncertainties, we find that there is reasonable agreement between data and the TL prediction in the invariant mass and angular distributions. However, the TL predictions for the transverse-energy spectra remain systematically harder than the data. The residual difference would presumably be smaller if next-to-leading order contributions were included, since additional final-state radiation can result in energy not counted as part of the photon plus two-jet system (out-of-cone energy, additional jets, etc.). Our implementation of K_T does not simulate these aspects of higher order radiation.

B. BREMSSTRAHLUNG VS. DIRECT PHOTON PRODUCTION

Prompt-photon production is often divided into two components, a direct component (represented in Figs. 1a, 1b) and a bremsstrahlung component (represented in Fig. 1c) [21]. Figures 1a and 1c, although topologically distinct, have the same initial and final states, and, in principle, interference effects make them inseparable. Keller and Owens

[21] pointed out that the gluon propagator in Fig. 1c gives rise to a different cos θ^* distribution in the parton center-of-mass frame, as compared with the quark propagator in Fig. 1a. By dividing the data into a bremsstrahlung-rich and a bremsstrahlung-poor component based on well-defined experimental cuts, one should be able to observe different cos θ^* distributions in the two samples. However, reference [21] used less restrictive photon cuts than is possible for the photon sample at CDF, and the difference between cos θ^* distributions using our analysis cuts is too small to distinguish. We therefore investigated ways to observe the two components using PYTHIA.

The PYTHIA prediction for photon production can be divided into a direct part, where the photon is produced by the subprocess $2 \rightarrow 2$ matrix element, and a bremsstrahlung part, where the photon is produced by a subsequent radiation of a photon off a quark. The simulation predicts that the bremsstrahlung process accounts for $(57 \pm 1(stat))\%$ of the total photon production. Fig. 9a shows that the invariant-mass distribution for bremsstrahlung production is harder than for direct photon production. The azimuthal separation between the two jets (Fig. 10) is also different for the two production processes. Taken together, these differences generally indicate that Jet2 is nearer the photon in bremsstrahlung events than in direct-photon events. This can be understood by observing that the photon in Fig. 1c will be correlated with the softer parton, while there is no such correlation in the direct case (Figs. 1a, 1b).

We now compare data with PYTHIA's predictions for bremsstrahlung and direct pro-

duction, as a test for the presence of the bremsstrahlung process. Comparison to the energy distributions (Fig. 9) yields poor results; no admixture of PYTHIA bremsstrahlung or direct photon production provides a consistent description of these spectra. This arises from the observation made earlier, that the photon and nominal jet E_T spectra in data are softer than the overall PYTHIA prediction. For some spectra, the bremsstrahlung prediction is softer than the direct prediction, while the opposite is true for others; in each case, the softer of the two predictions agrees better with the data. As noted earlier, the E_T spectrum for inclusive photons at the Tevatron is also softer than theoretical expectations. We conclude that, at least for the photon plus two-jet final state, the softer photon spectrum cannot be attributed simply to a larger than expected bremsstrahlung contribution. Although the mechanisms that cause the softer photon spectrum are not understood, we will assume that they do not affect the angular correlations to first order, and we use these as a sensitive probe of the bremsstrahlung fraction.

As discussed earlier, the azimuthal distributions are well described by the PYTHIA prediction (Fig. 4). The angular distributions for the bremsstrahlung and direct photon components are compared to data in Fig. 10. Neither process alone describes the $\Delta\phi$ distributions adequately, and the data require an admixture of the two processes. As a check, since the observed E_T spectra are softer than the PYTHIA predictions, we also tried weighting the PYTHIA sample so that the mass and E_T spectra matched the data. This resulted in slightly different $\Delta\phi$ predictions, but the data still require an admixture

of direct and bremsstrahlung contributions to fit the $\Delta\phi$ distributions.

Based on a least squares fit of the measured $\Delta\phi$ distributions to the two PYTHIA components, we find that a $(55 \pm 15)\%$ bremsstrahlung fraction best describes the data. The uncertainty is statistical. Allowing the distributions to vary within the systematic uncertainties, we find $(55 \pm 15^{+5}_{-10})\%$. Best agreement was achieved with $+1\sigma$ double-scatter background subtracted (22%), and a slightly smaller contribution from bremsstrahlung, resulting in an asymmetric uncertainty. The measured bremsstrahlung fraction is in good agreement with PYTHIA's prediction of $(57 \pm 1(stat))\%$.

The bremsstrahlung sample studied here is restricted by the selection cuts on E_T and isolation. Nevertheless, bremsstrahlung appears to account for a substantial fraction of our data sample, and thus is a nonnegligible contribution to inclusive prompt-photon production.

V. CONCLUSIONS

We have described the first analysis of photon plus two-jet events produced in $\bar{p}p$ collisions. The largest sources of experimental systematic uncertainty in kinematic distributions arise from the level of double-scatter background and the calorimeter energy scale.

Comparing to theoretical expectations, we find that the general features of the distributions are reproduced by both tree-level (TL) and PYTHIA predictions. A more

detailed comparison confirms that the three-body invariant-mass distribution is consistent with both predictions. The azimuthal distributions are also well described by PYTHIA, and within the bounds of TL uncertainties (in fragmentation and K_T). The jet E_T spectra are consistent with PYTHIA, but remain softer than TL even in light of theoretical uncertainties. The photon E_T spectrum is softer than either prediction and the difference cannot be attributed to experimental uncertainties or to any of the theoretical uncertainties considered in this analysis.

Comparing the angular distributions to PYTHIA's predictions for direct and bremsstrahlung photon production, we find that a mixture of direct and bremsstrahlung components describes the data better than either process alone. Within the framework of the PYTHIA calculation, our data support a bremsstrahlung component of $(55 \pm 15^{+5}_{-10})\%$ of the total, which compares well with the nominal PYTHIA prediction of $(57 \pm 1(stat))\%$. This constitutes the first attempt to study the hard bremsstrahlung component of photon production. We find no evidence of anomalous bremsstrahlung production relative to direct photon production.

We thank the Fermilab staff and the technical staffs of the participating institutions for their vital contributions. We also thank Stephane Keller, Jeff Owens and Torbjörn Sjöstrand for many valuable discussions. This work was supported by the U.S. Department of Energy and National Science Foundation; the Italian Istituto Nazionale di Fisica Nucleare; the Ministry of Education, Science and Culture of Japan; the Natural

Sciences and Engineering Research Council of Canada; the National Science Council of the Republic of China; and the A. P. Sloan Foundation.

References

[1] R.Brock *et al.*, Rev. Mod. Phys. **67**, 1 (1995).

A.D. Martin, W.S. Stirling, and R.G. Roberts, Phys Lett. **B 354**, 155 (1995).

[2] CDF collected 16 pb^{-1} in 1992 and 1993. A subsequent run (1994 to 1996) collected 80 pb^{-1}. Between the two periods of data taking, the trigger threshold for photons was raised from 16 to 23 GeV.

[3] H. Baer, J. Ohnemus, and J.F. Owens, Phys. Rev. D **42**, 61 (1990).

[4] T. Sjöstrand, Computer Physics Commun. 82, 74 (1994).

T. Sjöstrand, CERN-TH.7112, 1993.

[5] CDF Collaboration, F. Abe *et al.*, Phys. Rev. Lett. **73**, 2662 (1994) and reprint in Phys. Rev. Lett. **74**, 1891 (1995).

[6] J. Lamoureux, Proceedings of the XXXth Rencontres de Moriond on QCD and High Energy Hadronic Interactions, 59 (1995).

[7] CTEQ Collaboration, J. Huston *et al.*, Phys. Rev. D **51**, 6139 (1995).

[8] CDF Collaboration, F. Abe *et al.*, Nucl. Instrum. Methods A**267**, 272 (1988).

[9] CDF Collaboration, F. Abe *et al.*, Phys. Rev. D **48**, 2998 (1993).

[10] CDF Collaboration, F. Abe *et al.*, Phys. Rev. D **45**, 1448 (1992).

[11] CDF Collaboration, F. Abe *et al.*, Phys. Rev. Lett. **77**, 438 (1996).

[12] CTEQ Collaboration, J. Botts *et al.*, Phys. Rev. D **51**, 4763 (1995).

[13] F.E.Paige and S.D.Protopopescu, Report No. BNL-38034, 1986 (Unpublished).

[14] Events triggered on the $\bar{p}p$ bunch crossing at CDF occasionally include low-energy jet production. The parton E_T cut here is used mainly to facilitate jet/parton matching in order to avoid including jets from the underlying event into our simulation. Such events were subtracted from our data sample with the double-scatter background subtraction.

[15] CDF Collaboration, F. Abe *et al.*, Phys. Rev. D **50**, 5562 (1994).

[16] PYTHIA predictions of final-state color coherence effects are partially implemented through MSTJ(50). A mistake in PYTHIA5.7 is that this color coherence parameter is not implemented by default, although the documentation indicates otherwise. For this analysis, color coherence modeling was explicitly enabled by setting MSTJ(50)=3.

[17] A.D. Martin, R.G. Roberts, and W.J. Stirling, Phys. Lett. **B 387**, 419 (1996).

[18] CTEQ Collaboration, H.L. Lai *et al.*, Phys. Rev. D **55**, 1280 (1997).

[19] CDF Collaboration, F. Abe *et al.*, Phys. Rev. Lett. **75**, 608 (1995).

[20] D0 Collaboration, Abachi *et al.*, Phys. Rev. D **53**, 6000 (1996).

[21] S. Keller and J.F. Owens, Phys. Lett. **B 269**, 445 (1991).

List of Figures

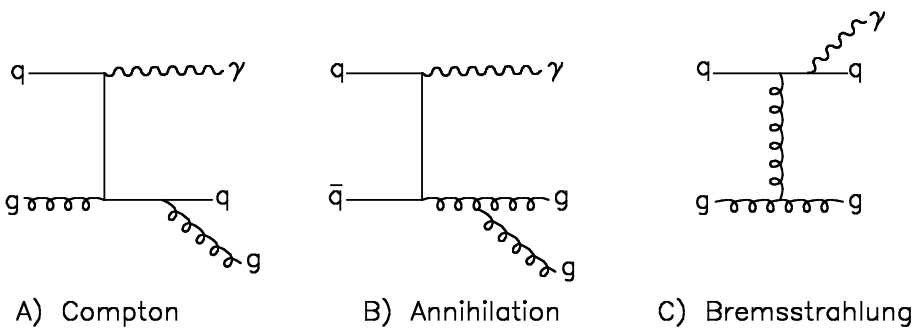

Figure 1: A) and B) are examples of direct-photon and two-parton production where the initial state defines the diagram as compton or annihilation production. C) is an example of bremsstrahlung production.

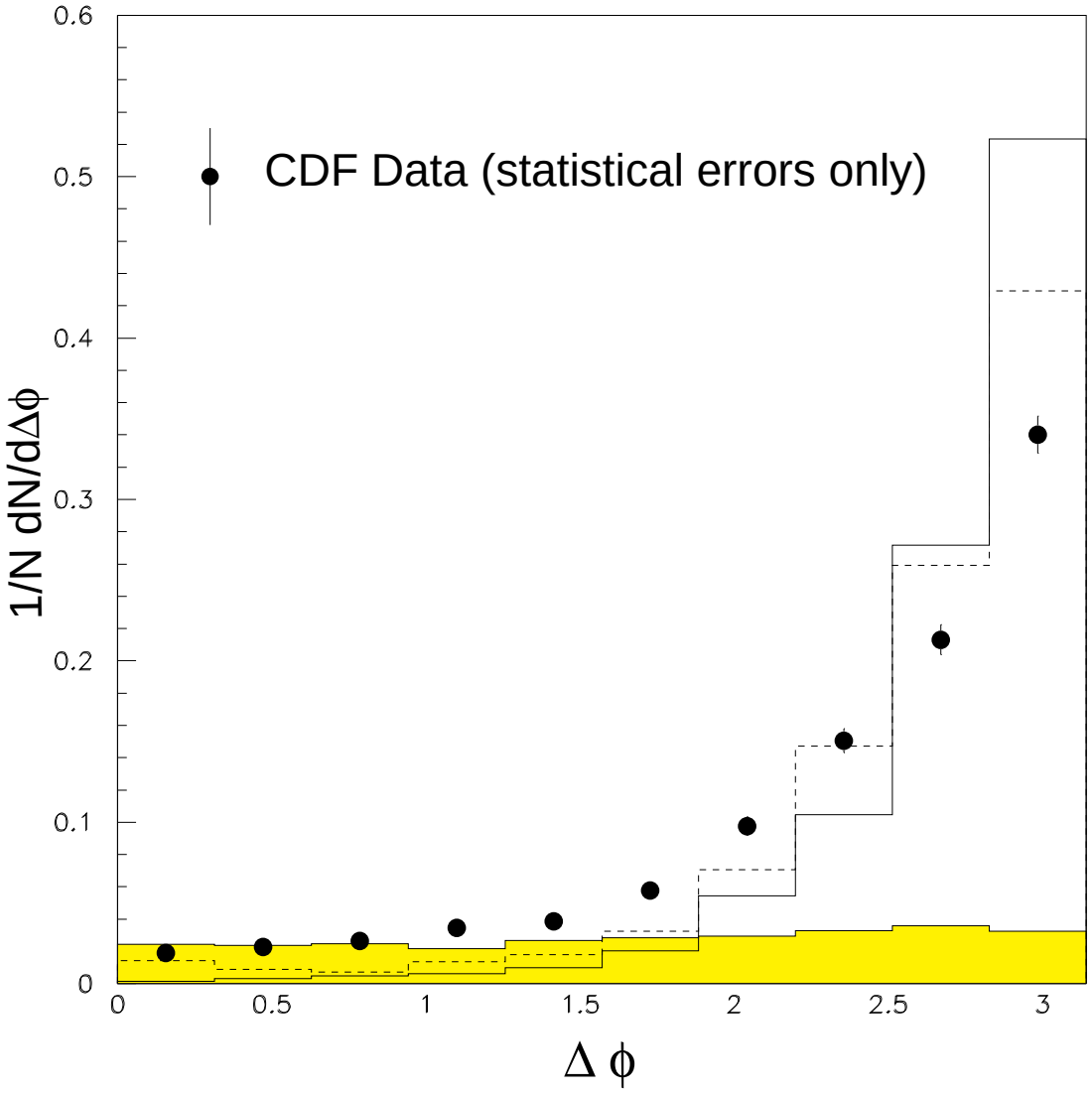

Figure 2: The difference in azimuthal angle, $\Delta\phi$, between the momentum-vector sum of the photon and leading jet, and the smaller E_T jet. The CDF data (points) are compared to the tree-level simulation (solid), PYTHIA (dashed) and double-scatter (shaded band normalized to 28%) prediction. Conservation of momentum in QCD events biases this angle towards π. The small-angle tail determines the amount of double-scatter background in the sample.

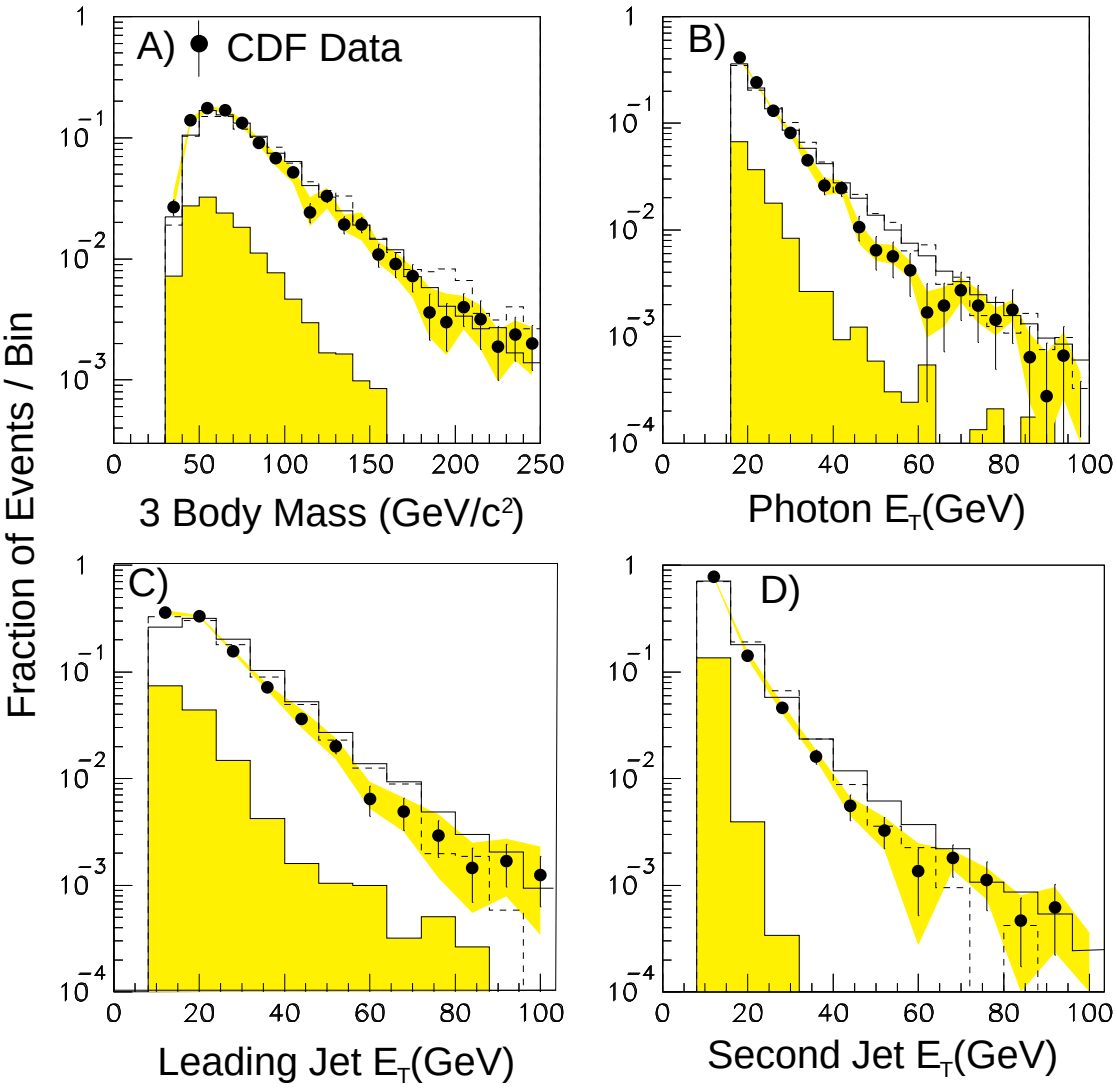

Figure 3: The measured invariant mass and transverse-energy spectra of the photon and jets (points) compared to predictions from tree-level (TL) simulation (solid) and PYTHIA (dashed). The shaded region at the bottom shows the shape of the double-scatter background that has been subtracted from the data. The experimental systematic uncertainty is shown as the shaded band surrounding the data.

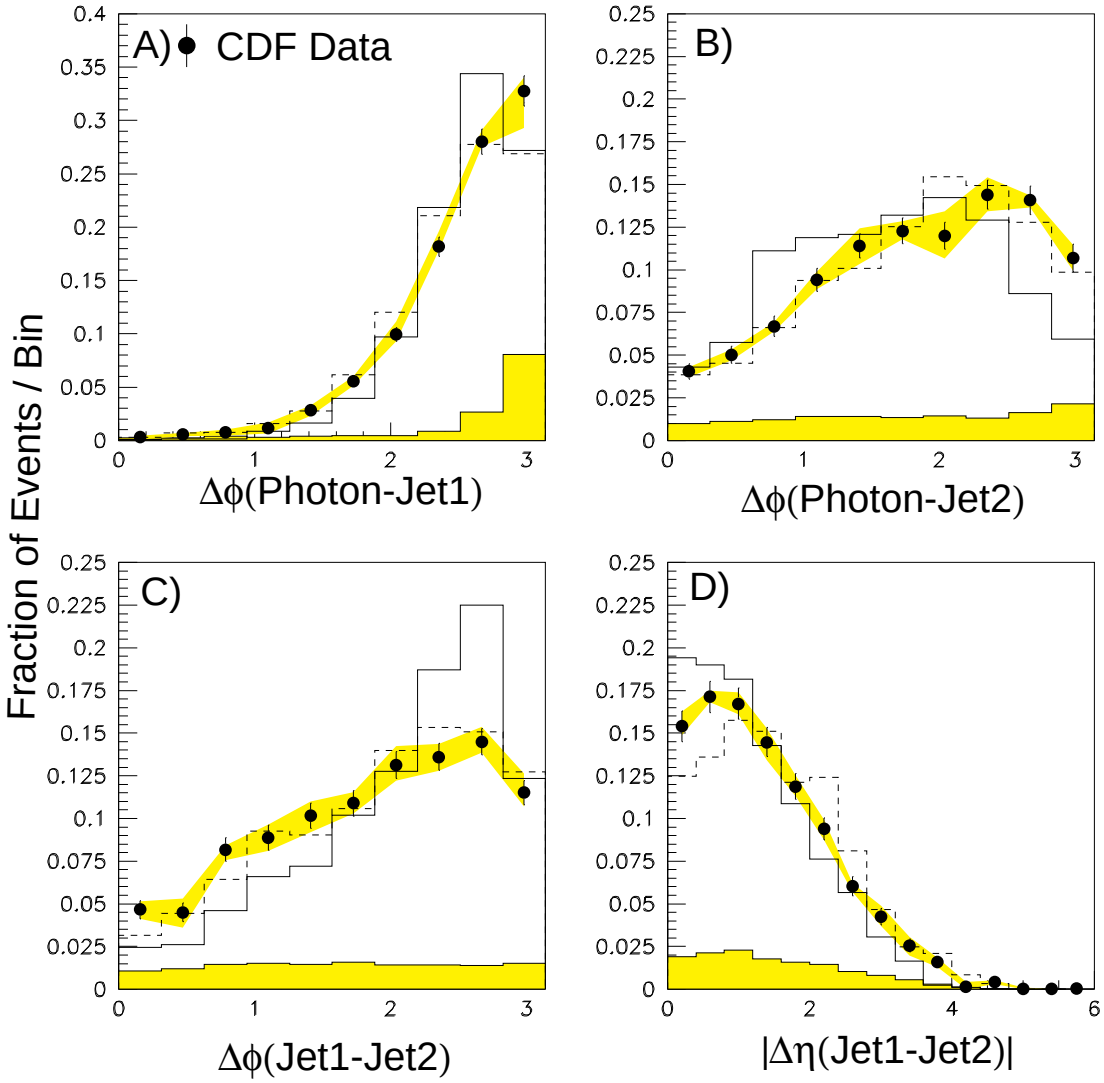

Figure 4: The measured $\Delta\phi$ and $|\Delta\eta|$ distributions (points) are compared to predictions from TL simulation (solid) and PYTHIA (dashed). The shaded region at the bottom shows the shape of the double-scatter background that has been subtracted from the data. The experimental systematic uncertainty is shown as the shaded band surrounding the data.

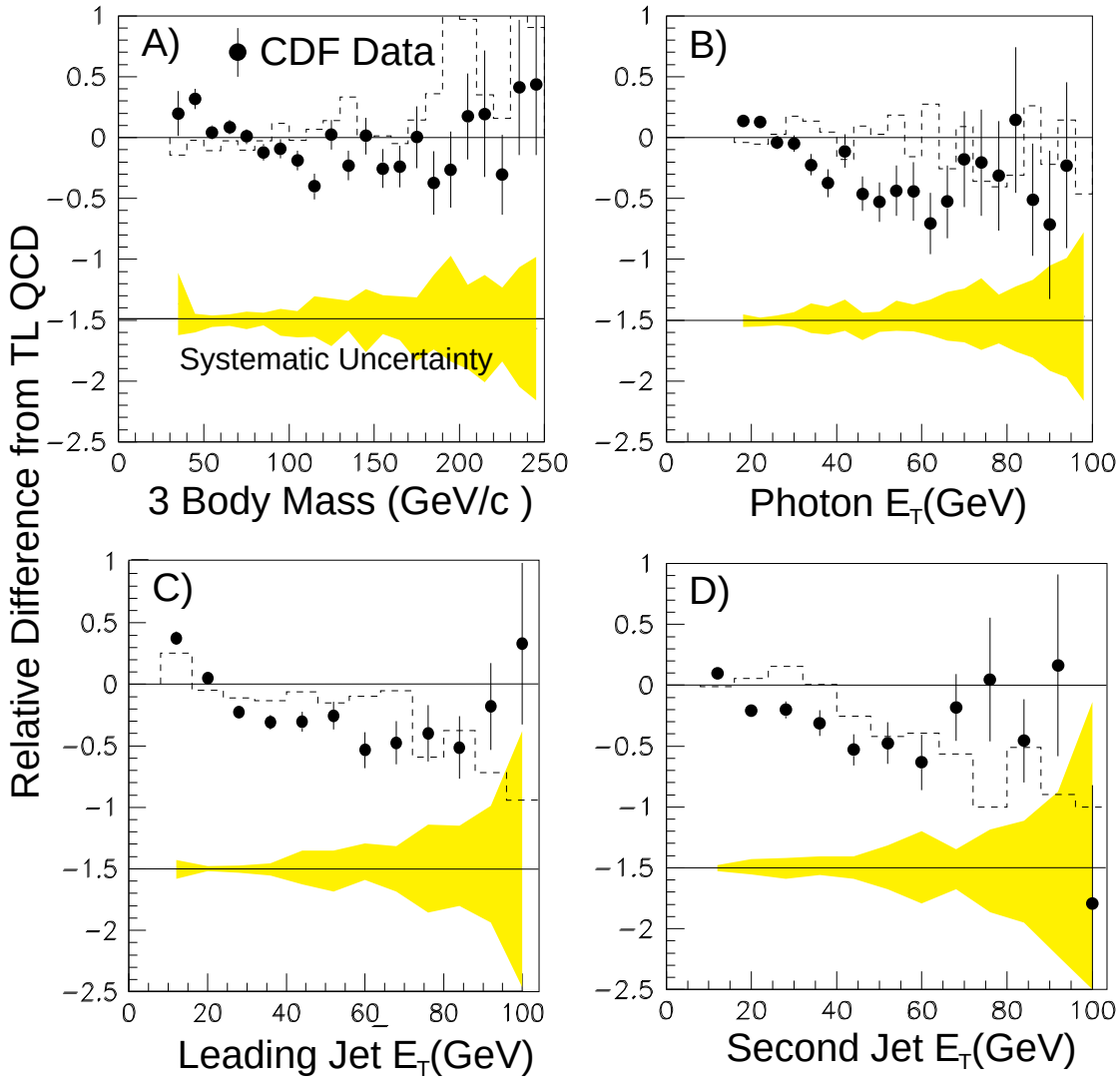

Figure 5: Residual plots for the measured invariant mass and transverse-energy spectra compared to the TL prediction ($Q^2 = p_{\mathrm{T}}^2$, $\Lambda_{\mathrm{QCD}} = 0.213$, CTEQ2M) including parton fragmentation and detector simulation. The data (points) are plotted as (data-TL)/TL. The PYTHIA comparison (PYTHIA-TL)/TL is also shown (dashed). The systematic uncertainty is shown as a shaded region offset (for clarity) by a factor of -1.5.

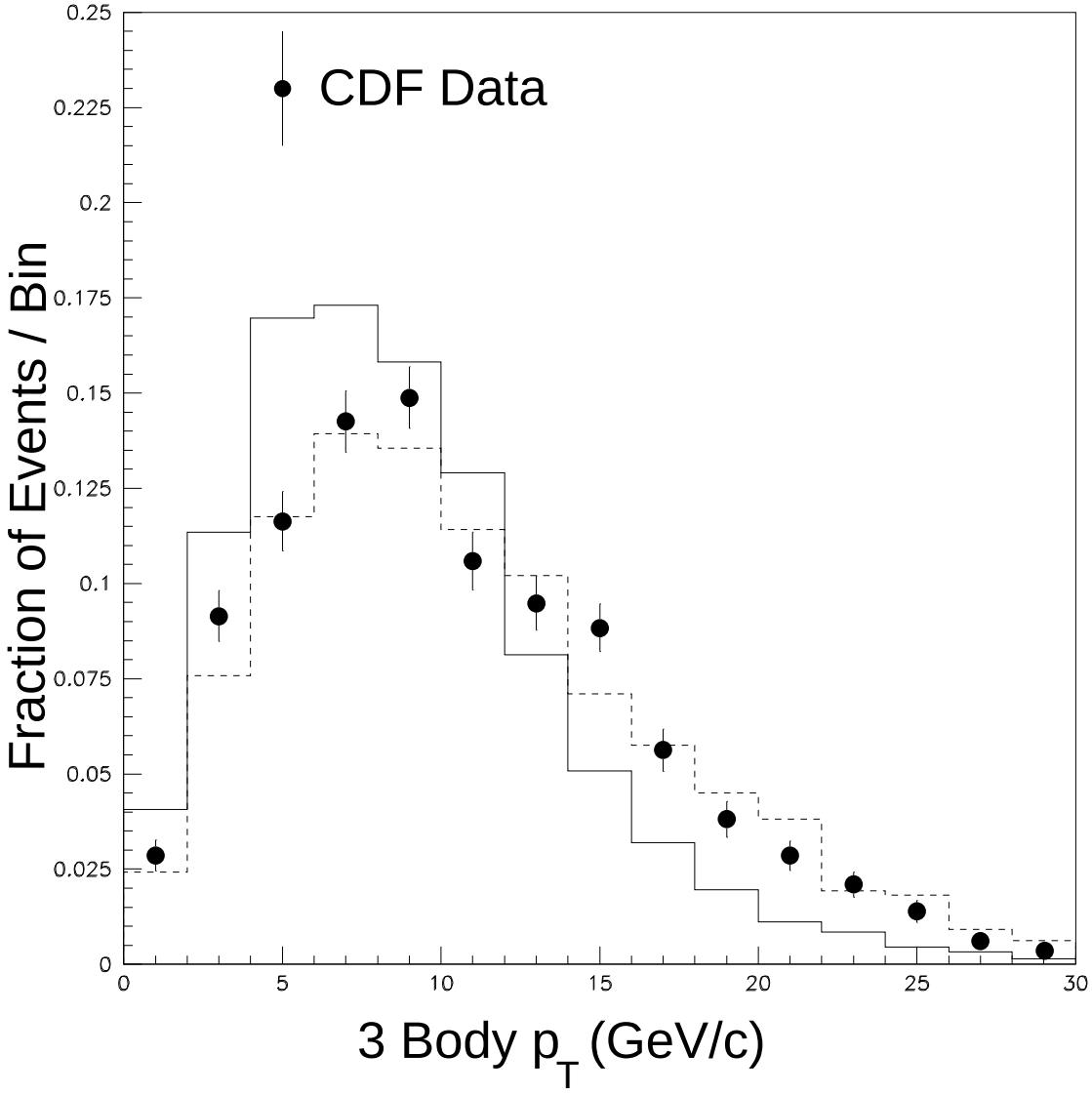

Figure 6: The three body p_{T} spectrum in the data (points) is compared to the TL (solid) and PYTHIA (dashed) predictions. PYTHIA includes a parton-shower model which adds a transverse boost (K_T) to the three-body system. The spectrum in the TL simulation reflects the detector-energy scale and resolution effects and fluctuations in the underlying event. In order to study K_T, a boost was added to the TL calculation so as to reproduce the shape observed here in the data.

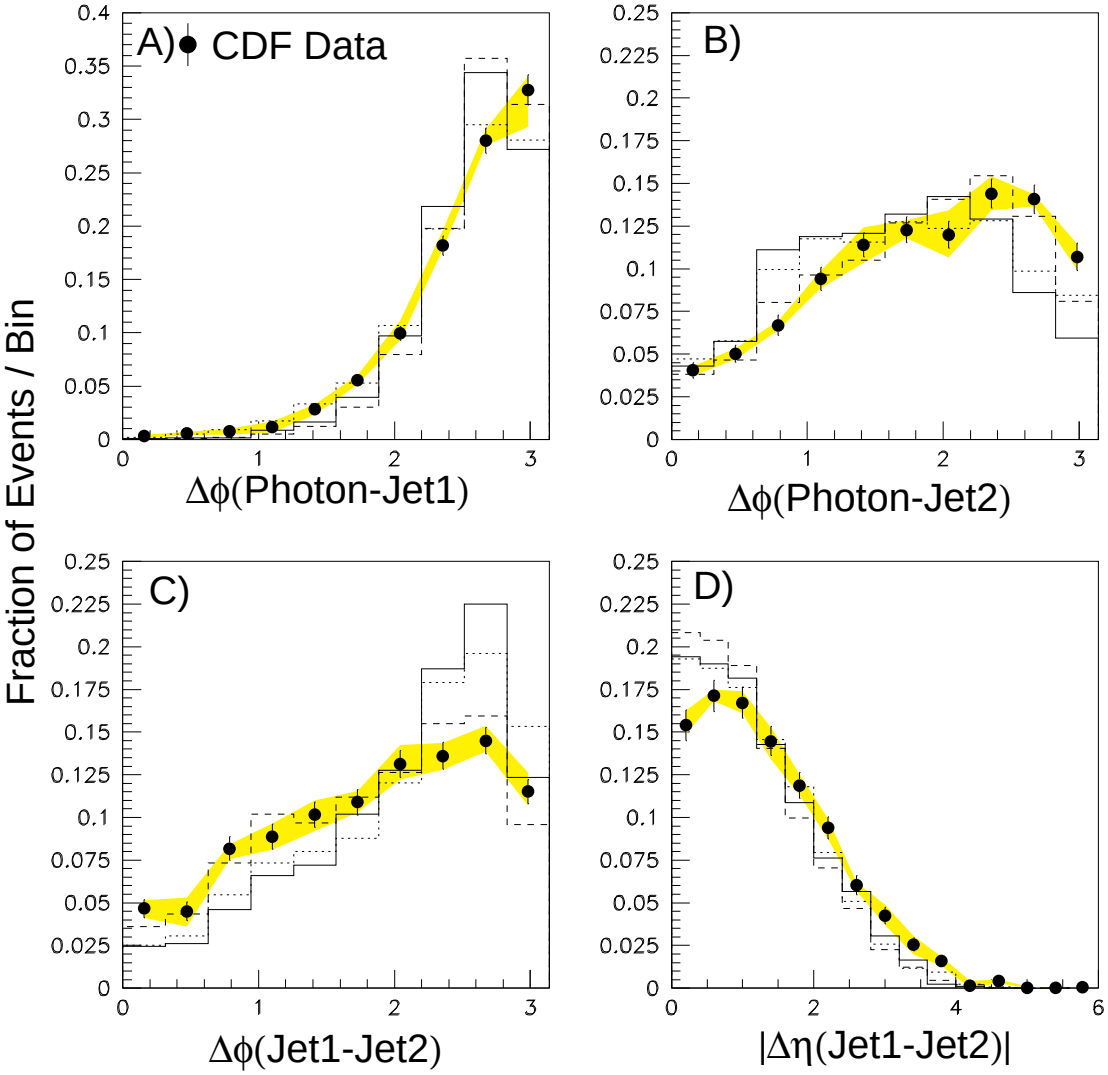

Figure 7: Comparisons of the measured $\Delta\phi$ and $|\Delta\eta|$ distributions (points) to the TL prediction (solid). Variations on the prediction due to the fragmentation uncertainty (dashed) and K_T smearing (dotted) are also shown.

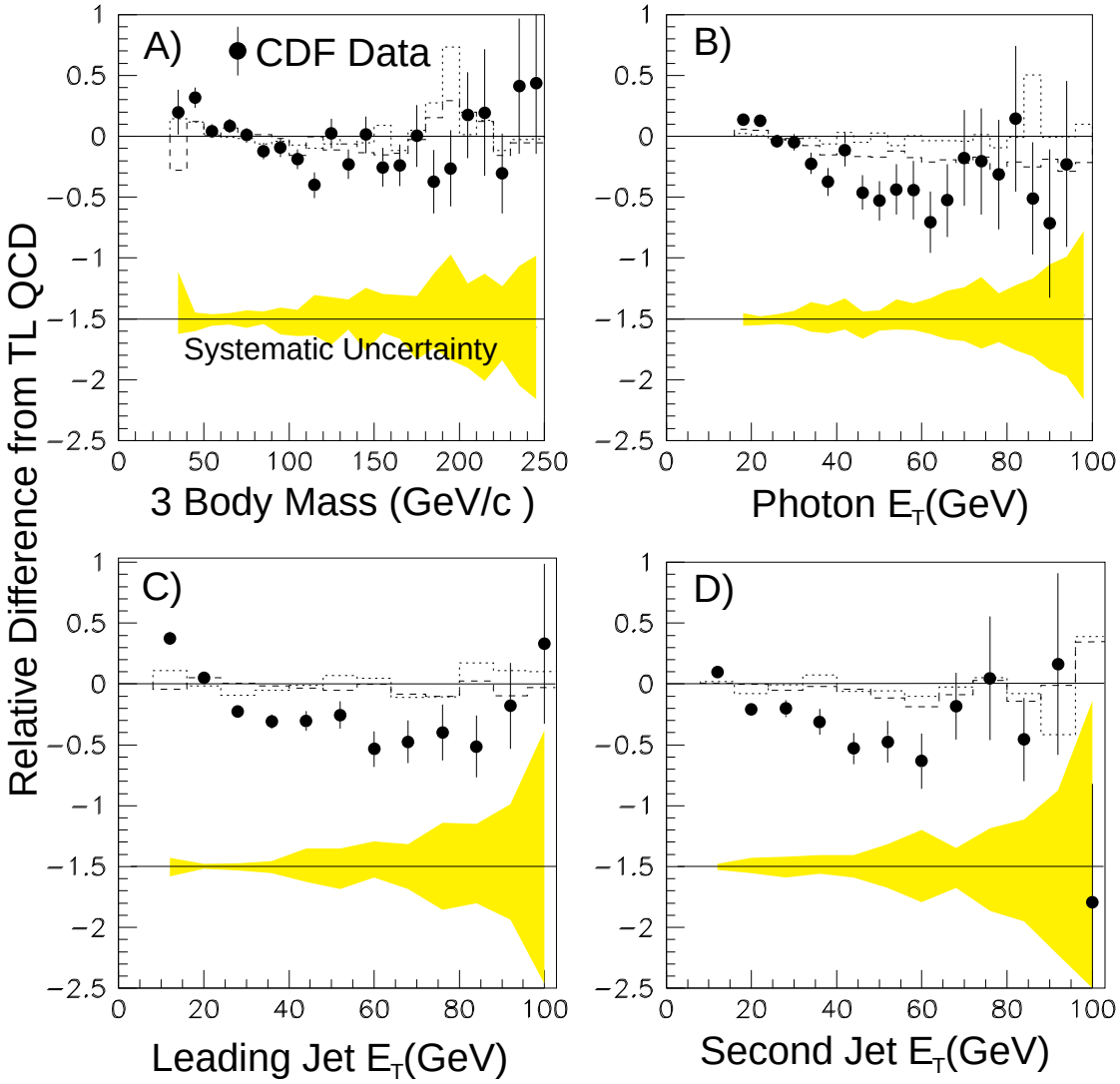

Figure 8: Residual plots for the measured invariant mass and transverse-energy spectra compared to the TL prediction ($Q^2 = p_{\mathrm{T}}^2$, $\Lambda_{\mathrm{QCD}} = 0.213$, CTEQ2M) including parton fragmentation and detector simulation. The data (points) are plotted as (data-TL)/TL. Variations on the prediction due to the fragmentation uncertainty (dashed) and K_T smearing (dotted) are also plotted as (Variation-TL)/TL. The systematic uncertainty is shown as a shaded region offset (for clarity) by a factor of -1.5.

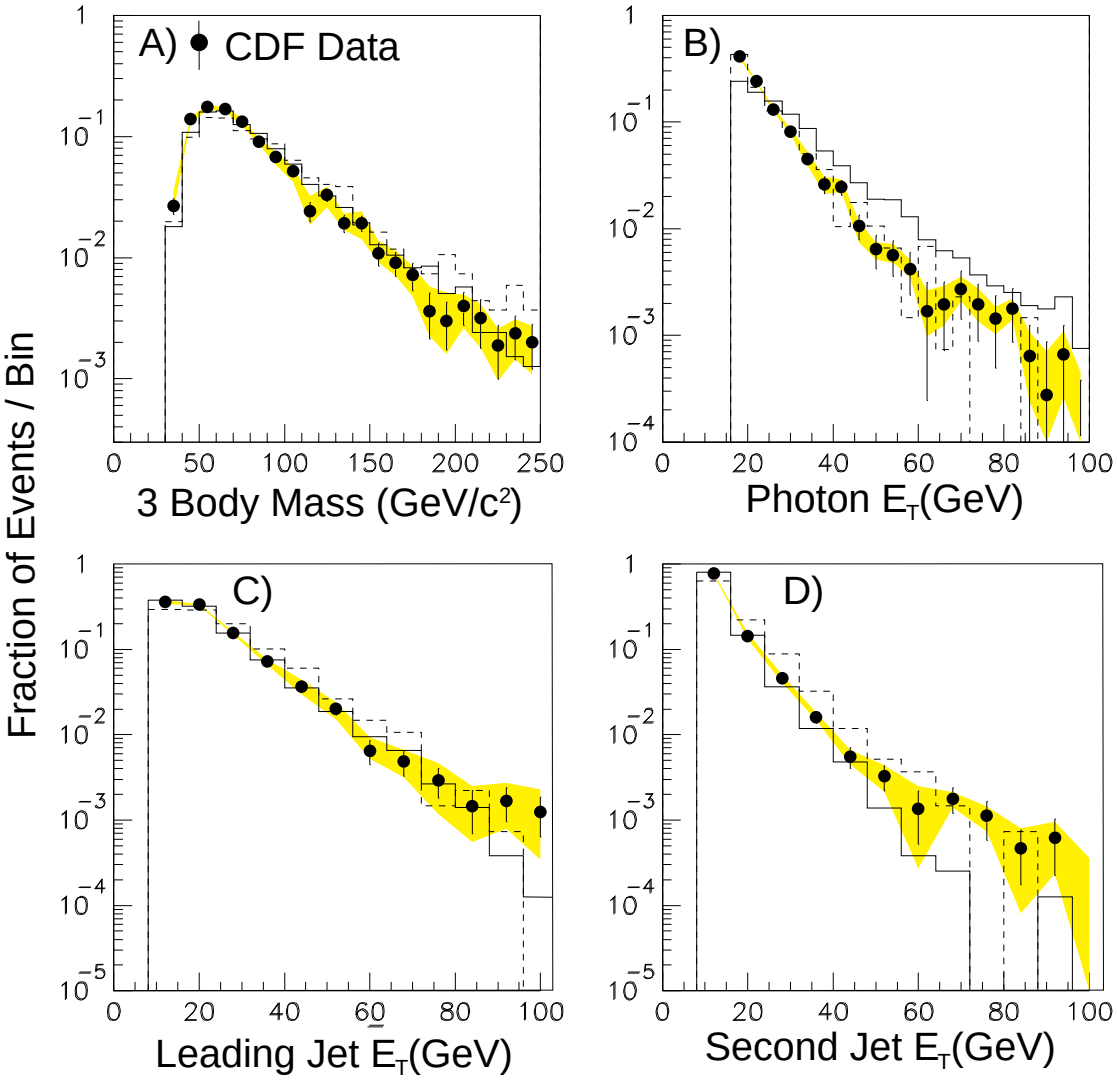

Figure 9: The measured invariant mass and transverse-energy spectra (points) are compared to the direct (solid) and bremsstrahlung (dashed) photon production parts of the PYTHIA prediction. The shaded band shows the systematic uncertainty.

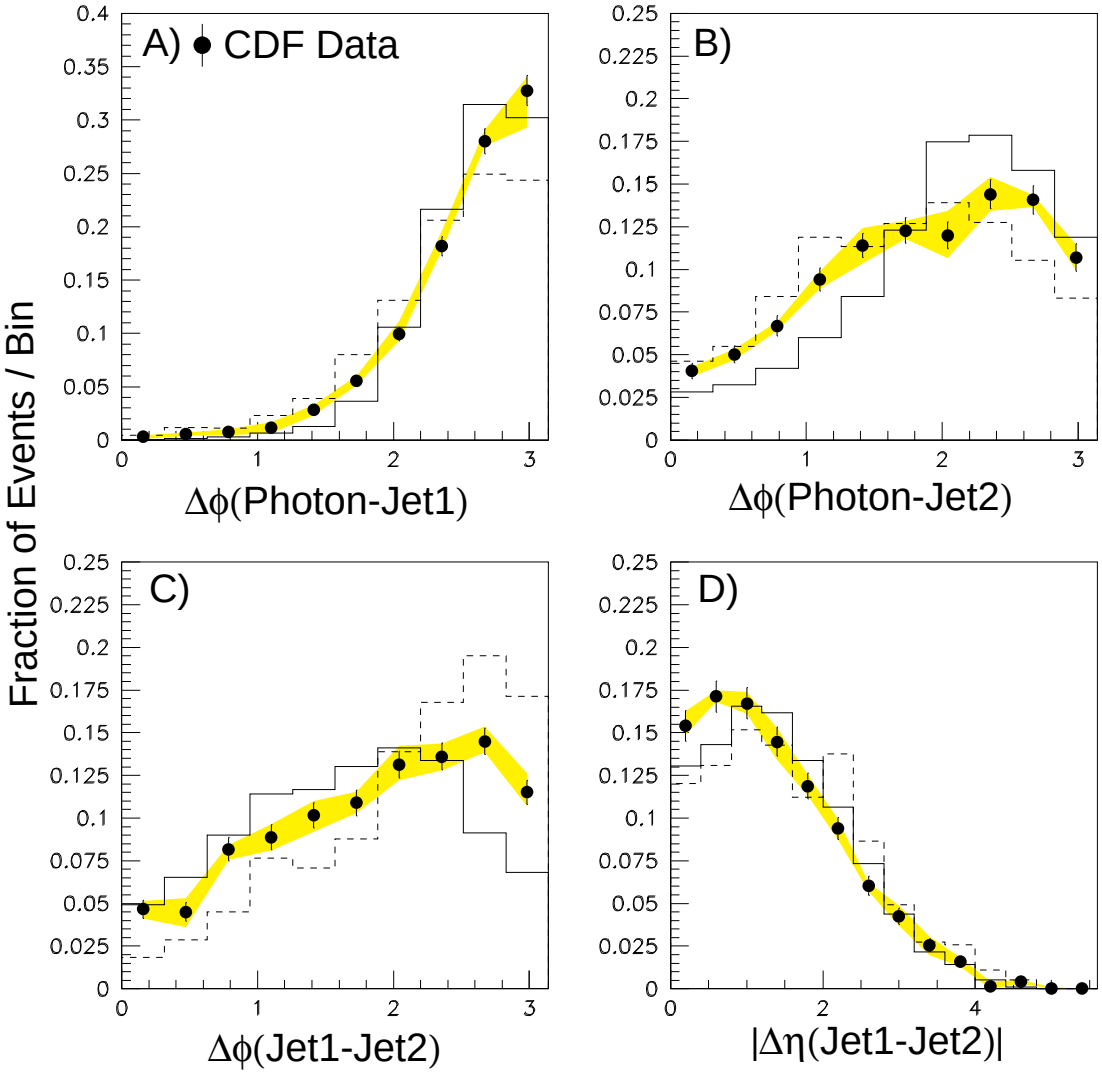

Figure 10: The measured $\Delta\phi$ and $|\Delta\eta|$ distributions (points) are compared to the direct (solid) and bremsstrahlung (dashed) photon production parts of the PYTHIA prediction. The shaded band shows the systematic uncertainty.